J|A|C|S ARTICLES

Published on Web 04/01/2009

Modeling Ethanol Decomposition on Transition Metals: A Combined Application of Scaling and Brønsted−Evans−Polanyi Relations

P. Ferrin,[†] D. Simonetti,[†] S. Kandoi,[†] E. Kunkes,[†] J. A. Dumesic,[†] J. K. Nørskov,[†,‡] and M. Mavrikakis*,[†]

Department of Chemical and Biological Engineering, University of Wisconsin—Madison, 1415 Engineering Drive, Madison, Wisconsin 53706, and Center for Atomic-Scale Materials Design, Department of Physics—Nano-DTU, Technical University of Denmark, DK-2800, Lyngby, Denmark

Received December 20, 2008; E-mail: manos@engr.wisc.edu

Abstract: Applying density functional theory (DFT) calculations to the rational design of catalysts for complex reaction networks has been an ongoing challenge, primarily because of the high computational cost of these calculations. Certain correlations can be used to reduce the number and complexity of DFT calculations necessary to describe trends in activity and selectivity across metal and alloy surfaces, thus extending the reach of DFT to more complex systems. In this work, the well-known family of Brønsted−Evans−Polanyi (BEP) correlations, connecting minima with maxima in the potential energy surface of elementary steps, in tandem with a scaling relation, connecting binding energies of complex adsorbates with those of simpler ones (e.g., C, O), is used to develop a potential-energy surface for ethanol decomposition on 10 transition metal surfaces. Using a simple kinetic model, the selectivity and activity on a subset of these surfaces are calculated. Experiments on supported catalysts verify that this simple model is reasonably accurate in describing reactivity trends across metals, suggesting that the combination of BEP and scaling relations may substantially reduce the cost of DFT calculations required for identifying reactivity descriptors of more complex reactions.

Introduction

The use of experimental surface science and catalysis techniques in conjunction with electronic structure theory to elucidate principles with which one can design new catalysts with desirable chemical properties has been a goal for decades. Rational catalyst design would use these principles to tailor a catalyst for specific process conditions and needs, increasing the overall efficiency of the process. In addition, using rational design may identify novel catalysts and processes to carry out challenging chemical transformations for new applications without extensive trial-and-error experimental testing.

Many challenges must be addressed, however, before rational catalyst design becomes feasible. One challenge is that of applying available theoretical methods to complex systems. In particular, density functional theory (DFT) has been successfully applied to develop reactivity trends for catalytic reactions,[1−8] such as water−gas shift,[9−11] ammonia synthesis,[12] preferential oxidation of CO in the presence of H_2,[13] methanation,[14] selective hydrogenation,[15] oxygen reduction reaction,[16−20] and ethylene epoxidation,[21] among others. However, because of its intense computational requirements for even relatively small systems,

[†] University of Wisconsin—Madison.
[‡] Technical University of Denmark.

(1) Alcala, R.; Greeley, J.; Mavrikakis, M.; Dumesic, J. A. *J. Chem. Phys.* **2002**, *116*, 8973.
(2) Kandoi, S.; Greeley, J.; Sanchez-Castillo, M. A.; Evans, S. T.; Gokhale, A. A.; Dumesic, J. A.; Mavrikakis, M. *Top. Catal.* **2006**, *37*, 17.
(3) Nørskov, J. K.; Bligaard, T.; Logadottir, A.; Bahn, S.; Hansen, L. B.; Bollinger, M.; Bengaard, H.; Hammer, B.; Sljivancanin, Z.; Mavrikakis, M.; Xu, Y.; Dahl, S.; Jacobsen, C. J. H. *J. Catal.* **2002**, *209*, 275.
(4) Kitchin, J. R.; Nørskov, J. K.; Barteau, M. A.; Chen, J. G. *J. Chem. Phys.* **2004**, *120*, 10240.
(5) Toulhoat, H.; Raybaud, P. *J. Catal.* **2003**, *216*, 63.
(6) Michaelides, A.; Liu, Z. P.; Zhang, C. J.; Alavi, A.; King, D. A.; Hu, P. *J. Am. Chem. Soc.* **2003**, *125*, 3704.
(7) Pallassana, V.; Neurock, M. *J. Catal.* **2000**, *191*, 301.
(8) Greeley, J.; Mavrikakis, M. *Nat. Mater.* **2004**, *3*, 810.
(9) Gokhale, A. A.; Dumesic, J. A.; Mavrikakis, M. *J. Am. Chem. Soc.* **2008**, *130*, 1402.
(10) Grabow, L. C.; Gokhale, A. A.; Evans, S. T.; Dumesic, J. A.; Mavrikakis, M. *J. Phys. Chem. C* **2008**, *112*, 4608.
(11) Schumacher, N.; Boisen, A.; Dahl, S.; Gokhale, A. A.; Kandoi, S.; Grabow, L. C.; Dumesic, J. A.; Mavrikakis, M.; Chorkendorff, I. *J. Catal.* **2005**, *229*, 265.
(12) Jacobsen, C. J. H.; Dahl, S.; Clausen, B. S.; Bahn, S.; Logadottir, A.; Nørskov, J. K. *J. Am. Chem. Soc.* **2001**, *123*, 8404.
(13) Alayoglu, S.; Nilekar, A. U.; Mavrikakis, M.; Eichhorn, B. *Nat. Mater.* **2008**, *7*, 333.
(14) Andersson, M. P.; Bligaard, T.; Kustov, A.; Larsen, K. E.; Greeley, J.; Johannessen, T.; Christensen, C. H.; Nørskov, J. K. *J. Catal.* **2006**, *239*, 501.
(15) Studt, F.; Abild-Pedersen, F.; Bligaard, T.; Sorensen, R. Z.; Christensen, C. H.; Nørskov, J. K. *Science* **2008**, *320*, 1320.
(16) Nilekar, A. U.; Mavrikakis, M. *Surf. Sci.* **2008**, *602*, L89.
(17) Filhol, J. S.; Neurock, M. *Angew. Chem.-Int. Ed.* **2006**, *45*, 402.
(18) Stamenkovic, V.; Mun, B. S.; Mayrhofer, K. J. J.; Ross, P. N.; Markovic, N. M.; Rossmeisl, J.; Greeley, J.; Nørskov, J. K. *Angew. Chem.-Int. Ed.* **2006**, *45*, 2897.
(19) Zhang, J. L.; Vukmirovic, M. B.; Sasaki, K.; Nilekar, A. U.; Mavrikakis, M.; Adzic, R. R. *J. Am. Chem. Soc.* **2005**, *127*, 12480.
(20) Zhang, J. L.; Vukmirovic, M. B.; Xu, Y.; Mavrikakis, M.; Adzic, R. R. *Angew. Chem.-Int. Ed.* **2005**, *44*, 2132.
(21) Linic, S.; Jankowiak, J.; Barteau, M. A. *J. Catal.* **2004**, *224*, 489.

10.1021/ja8099322 CCC: $40.75

DFT has generally been used only to study relatively well-characterized systems and comparatively simple reaction mechanisms.

To simplify this computational cost problem, correlations have been developed to reduce complex phenomena to more tractable problems. One of the chief examples of this approach is the Brønsted−Evans−Polanyi (BEP) correlation that relates the transition-state energy of an elementary step to the energy of the corresponding final state or reaction enthalpy in a linear way.[3,22−26] A second linear correlation relates the binding energy of molecular adsorbates on a given surface to the binding energy of the atom through which it adsorbs on the same surface.[15,27,28] The combination of these two linear correlations is potentially powerful, because it allows the determination of both the minima (through the so-called scaling correlation) and the maxima (through the BEP relation) of the potential energy surface (PES) for a given reaction on any transition metal surface, with the only inputs being the parameters for the two correlations and the binding energy of atomic adsorbates on the surface. Here, we illustrate, for the first time, the power of this combined approach, using ethanol decomposition on transition metals as a case study.

The decomposition of ethanol on metal surfaces is of both fundamental and applied interest.[29] The interaction of ethanol with metal surfaces is key to ethanol steam reforming, direct ethanol fuel cells, and many other industrially relevant reactions. Additionally, ethanol is a good model molecule for selectivity studies; it is the simplest molecule that contains both C−C and C−O single bonds. The ease of cleavage of each of these bonds on different metal surfaces determines the relative selectivity of products.[30] Facile C−C bond breaking leads to the production of hydrogen through ethanol reforming,[31] whereas C−O bond breaking leads to the production of alkanes.[32] Depending on the application, either of these scenarios may be desirable; thus, there is a need to be able to predict and ultimately control the relative rates of these two reactions on various metal surfaces. Toward this end, several studies have looked at the cleavage of these two bonds using both surface science and density functional theory on selected facets of several metals, including Pt,[30,33−38] Ru,[39] Rh,[40,41] and others.[42,43]

Herein, we use the two types of correlations mentioned above to develop a set of binding energies of relevant intermediates and transition state energies for the respective elementary steps in ethanol decomposition on the close-packed facets of 10 metals (Cu, Pt, Pd, Ni, Ir, Rh, Co, Os, Ru, and Re), using only the binding energy of C, O, CO, and H on these metals as input. Using these comparatively few DFT inputs, the potential energy surface for C−O and C−C bond breaking in ethanol is produced on these 10 metals. Through a simplified kinetic model described herein, we then qualitatively predict trends in ethanol decomposition activity and selectivity on six of these metals: Cu, Pt, Pd, Ir, Rh, and Ru. These trends are subsequently validated through experimental activity testing of the appropriate supported metal catalysts.

Methods

Computational Methods. The binding energy of different adsorbates on each surface is calculated by employing density functional theory using DACAPO, a total energy code.[44,45] A periodic 3 × 3 unit cell (corresponding to 1/9 ML coverage of each adsorbate) with three layers of metal atoms for each slab and at least five equivalent layers of vacuum between successive slabs is used throughout this study. Metal atoms are kept fixed at their optimized bulk positions, as selected calculations showed that surface relaxation has only small effects on the energetics of the close-packed systems studied.[1] The (111) facet of the face-centered cubic metals (Cu, Pt, Pd, Ni, Ir, and Rh) and the (0001) surface of the hexagonal close-packed metals (Co, Os, Ru, and Re) is used. Spin-polarized calculations were performed for adsorption on Co and Ni. Adsorption is allowed on only one of the two exposed surfaces, and the dipole moment is adjusted accordingly. Ionic cores are described by ultrasoft pseudopotentials.[46] The Kohn−Sham one-electron states are expanded in a series of plane waves with an energy cutoff of 25 Ry. On the basis of the convergence of total energies, the surface Brillouin zone is sampled at six special Chadi−Cohen k-points for all metals studied, with the exception of Cu, where 18 special k-points were necessary.[47] The exchange-correlation energy and potential are described self-consistently, using the PW91 form of the generalized gradient approximation (GGA).[48] The electron density is determined by iterative diagonalization of the Kohn−Sham Hamiltonian, Fermi population of the Kohn−Sham states ($k_BT = 0.1$ eV), and Pulay mixing of the resulting electronic density. All total energies have been extrapolated to $k_BT = 0$ eV.

Experimental Methods. Carbon-supported Cu, Pt, Pd, Ru, Ir, and Rh catalysts were prepared by incipient wetness impregnation of carbon black (Vulcan XC-72) with aqueous solutions of $Cu(NO_3)_2$, $H_2PtCl_6 \cdot 6H_2O$, $PdCl_2$, $Ru(NO)(NO_3)_3$, $IrCl_3$, and $RhCl_3$, respectively, to give catalysts with nominal metal loadings of 10% Cu, 3 wt % Pt, 5 wt % Pd, 5 wt % Ru, 3 wt % Ir, and 5 wt % Rh. The support was dried in air for 12 h at 373 K prior to impregnation, and 1.7 g of solution was used per gram of support. After

(22) Barteau, M. A. *Catal. Lett.* **1991**, *8*, 175.
(23) Bligaard, T.; Nørskov, J. K.; Dahl, S.; Matthiesen, J.; Christensen, C. H.; Sehested, J. *J. Catal.* **2004**, *224*, 206.
(24) Cheng, J.; Hu, P.; Ellis, P.; French, S.; Kelly, G.; Lok, C. M. *J. Phys. Chem. C* **2008**, *112*, 1308.
(25) Logadottir, A.; Rod, T. H.; Nørskov, J. K.; Hammer, B.; Dahl, S.; Jacobsen, C. J. H. *J. Catal.* **2001**, *197*, 229.
(26) Xu, Y.; Ruban, A. V.; Mavrikakis, M. *J. Am. Chem. Soc.* **2004**, *126*, 4717.
(27) Jones, G.; Bligaard, T.; Abild-Pedersen, F.; Nørskov, J. K. *J. Phys. Condens. Matter* **2008**, *20*, 064239.
(28) Abild-Pedersen, F.; Greeley, J.; Studt, F.; Rossmeisl, J.; Munter, T. R.; Moses, P. G.; Skulason, E.; Bligaard, T.; Nørskov, J. K. *Phys. Rev. Lett.* **2007**, *99*, 016105.
(29) Mavrikakis, M.; Barteau, M. A. *J. Mol. Catal. A* **1998**, *131*, 135.
(30) Alcala, R.; Mavrikakis, M.; Dumesic, J. A. *J. Catal.* **2003**, *218*, 178.
(31) Cortright, R. D.; Davda, R. R.; Dumesic, J. A. *Nature* **2002**, *418*, 964.
(32) Huber, G. W.; Chheda, J. N.; Barrett, C. J.; Dumesic, J. A. *Science* **2005**, *308*, 1446.
(33) Lee, A. F.; Gawthrope, D. E.; Hart, N. J.; Wilson, K. *Surf. Sci.* **2004**, *548*, 200.
(34) Cong, Y.; vanSpaendonk, V.; Masel, R. I. *Surf. Sci.* **1997**, *385*, 246.
(35) Davda, R. R.; Alcala, R.; Shabaker, J.; Huber, G.; Cortright, R. D.; Mavrikakis, M.; Dumesic, J. A. *Sci. Technol. Catal.* **2003**, *145*, 79.
(36) Rajumon, M. K.; Roberts, R. S.; Wang, F.; Wells, P. B. *J. Chem. Soc. Faraday Trans.* **1998**, *94*, 3699.
(37) Sexton, B. A.; Rendulic, K. D.; Hughes, A. E. *Surf. Sci.* **1982**, *121*, 181.
(38) Wang, H. F.; Liu, Z. P. *J. Am. Chem. Soc.* **2008**, *130*, 10996.
(39) Kandoi, S, Dumesic, J. A.; Mavrikakis, M., manuscript to be submitted.
(40) Houtman, C. J.; Barteau, M. A. *J. Catal.* **1991**, *130*, 528.
(41) Vesselli, E.; Baraldi, A.; Comelli, G.; Lizzit, S.; Rosei, R. *ChemPhysChem* **2004**, *5*, 1133.
(42) Weststrate, C. J.; Ludwig, W.; Bakker, J. W.; Gluhoi, A. C.; Nieuwenhuys, B. E. *ChemPhysChem* **2007**, *8*, 932.
(43) Bowker, M.; Holroyd, R. P.; Sharpe, R. G.; Corneille, J. S.; Francis, S. M.; Goodman, D. W. *Surf. Sci.* **1997**, *370*, 113.
(44) Greeley, J.; Nørskov, J. K.; Mavrikakis, M. *Annu. Rev. Phys. Chem.* **2002**, *53*, 319.
(45) Hammer, B.; Hansen, L. B.; Nørskov, J. K. *Phys. Rev. B* **1999**, *59*, 7413.
(46) Vanderbilt, D. *Phys Rev B* **1990**, *41*, 7892.
(47) Chadi, D. J.; Cohen, M. L. *Phys Rev B* **1973**, *8*, 5747.
(48) Perdew, J. P.; Chevary, J. A.; Vosko, S. H.; Jackson, K. A.; Pederson, M. R.; Singh, D. J.; Fiolhais, C. *Phys Rev B* **1992**, *46*, 6671.

Table 1. Catalyst Parameters Determined from Experiments and Experimental Conversion for Ethanol Decomposition

metal	metal loading	μmol sites/g catalyst	dispersion (%)	overall ethanol conversion (%)	conversion to C_2H_6(%)	conversion to CO/CH_4(%)
Cu	0.10	39	2.5	0	0	0
Pt	0.05	130	50.7	5.2	0.09	5.1
Pd	0.03	120	42.6	2.3	<0.01	2.3
Ir	0.05	78	30.0	2.2	0.06	2.2
Rh	0.03	120	41.1	4.2	<0.01	4.2
Ru	0.05	200	40.4	15.1	0.12	15.0

impregnation, the catalyst were dried at 403 K for 12 h in air. The adsorption uptakes of CO (N_2O on Cu) at 300 K (369K for Cu) were measured on a standard gas adsorption apparatus described elsewhere.[49] The number of catalytic sites was taken to be equal to the irreversible CO (O for Cu) uptake. Prior to reaction kinetics or gas adsorption measurements (i.e., CO or N_2O chemisorption), the catalysts were reduced in H_2 [180 cm^3 (STP) min^{-1}] at 723 K (523 K for Cu) (0.5 K min^{-1}) for 2 h. The dispersion values for the six catalysts tested are shown in Table 1.

The reactor used for kinetics studies of ethanol conversion was a 6.3 mm (0.25 in.) outer diameter stainless steel tube with a wall thickness of 0.71 mm (0.028 in.). A bed consisting of fresh powder catalyst (100−260 mg) mixed with an equal volume of crushed fused SiO_2 granules (SiO_2:catalyst mass ratio equal to 4:1) was loaded between a quartz wool plug and fused SiO_2 granules (−4+16 mesh; Sigma Aldrich). The reactor was heated with a furnace consisting of a close-fitting aluminum block heated externally by a well-insulated furnace (1450 W/115 V, Applied Test Systems series 3210), and a K-type thermocouple (Omega) was attached to the outside of the reactor to measure reactor temperature, which was controlled with a 1600-series type temperature controller (Dwyer Instruments). Reactor temperature was kept constant at 523 K for all experiments. Liquid ethanol (200 proof; Sigma Aldrich) was introduced into the reactor with a H_2 cofeed in a down-flow configuration. The liquid ethanol flow rate was controlled with an HPLC pump (Alltech model 301), and a syringe needle (Hamilton; point 5 tip) was used to introduce droplets of the feed into the reactor where vaporization occurs. The H_2 flow was controlled with a Brooks 5850 model mass-flow controller. The H_2:ethanol molar ratio was 4:1 for all experiments, and the weight hourly space velocity (WHSV) was calculated as the hourly mass flow rate of ethanol divided by the total amount of catalyst in the reactor. The effluent liquid was condensed in a gas−liquid separator and drained for gas chromatograph (GC) analysis with a Shimadzu GC-2010 equipped with an FID detector and Rtx-5 column. The effluent gas stream was analyzed for CO, CO_2, and light alkanes (C_1−C_3) using an HP-5890 GC with thermal conductivity detector (TCD) and a Haysep DB 100/120 column (Alltech). Reaction kinetics data were collected for 8 h on stream for each set of reaction conditions to ensure that the catalyst system reached steady state. Experimental turnover frequencies (TOF) were calculated on the basis of the amount of ethane (for C−O cleavage) and CO (for C−C cleavage) produced in the reactor and the number of sites determined with the adsorption uptake experiments. Following an initial start-up period, the overall conversion of ethanol on each catalyst tested remained stable throughout the 8 h on stream, indicating no deactivation of the catalyst particles over the course of the study.

Model Description. Using the binding energies of ethanol-derived adsorbates on Ru(0001) from Kandoi et al.,[39] we can extend our model to any other transition metal surface with which ethanol may interact. Abild-Pedersen, et al.[28] found that the binding energies of any species AH_x (A = O, C, N, S) linearly correlates with the binding energy of the atom A, such that

$$\Delta E^{AH_x} = \gamma(x)\Delta E^{A} + \xi$$

where ΔE^{A} is the binding energy of atomic species A, ΔE^{AH_x} is the binding energy of the AH_x species, and ξ and γ are the correlation parameters, varying with different adsorbates. $\gamma(x)$ is a well-defined function of the bonding characteristics of AH_x and is given to a good approximation by

$$\gamma(x) = \frac{x_{max} - x}{x_{max}}$$

where x_{max} is the number of H atoms needed to bind to the atom A (through which the adsorbate binds to the surface) so as to make a closed-shell gas phase species $AH_{x_{max}}$ (e.g., $x_{max} = 4$ for C). This result is due to the change in electron density between the central atom A and the surface when bonded to other atoms, in this case H. Neglecting back-bonding of π bonds, a similar argument can be made that the electron density will change in a similar way for other groups bound to the central A atom (such as CH_3 or OH). Thus, this method can be used to correlate the binding energies of many adsorbates to metal surfaces. One can estimate the binding energy of an adsorbate (AH_x) on any metal surface based on a calculated value of the binding energy of that adsorbate (AH_x) on one surface (so as to fix ξ) and the binding energy of the atom (A) through which the adsorbate is bound to the surface of interest. By using the binding energies of all ethanol-derived intermediates calculated for Ru(0001)[39] and the binding energy of C, O, and H on the remaining transition metals, we can find the binding energies of all 47 intermediates relevant to ethanol decomposition on a number of metal surfaces. To check the validity of this correlation for ethanol decomposition intermediates, the binding energies found through this correlation for species on Pt(111) were compared with direct DFT values taken from ref 30 (see Figure 1). The mean absolute error for all intermediates was 0.21 eV. Given that the inherent error in DFT is on the order of 0.1−0.2 eV, this means that the use of the scaling relation does not add significantly to the uncertainty in the binding energy of intermediates for ethanol decomposition.

Previous work has shown a BEP-type relation for C−C and C−O cleavage for species with a C−C−O backbone, independent of the degree of hydrogenation, on Pt(111).[30] A similar correlation has been found on Ru(0001),[39] suggesting that this correlation is also independent of the metal surface. This correlation, relating transition state energy to final state energy, is shown for both metals in Figure 2. The combination of these two simple correlations—first, the use of the scaling relations to estimate the binding energies of all

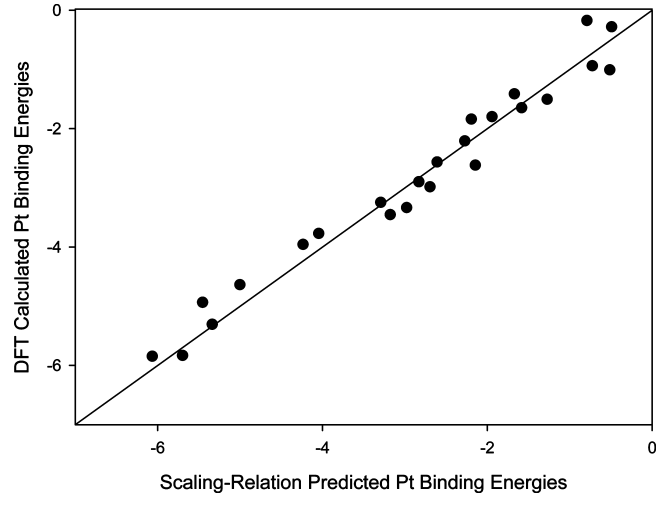

Figure 1. Binding energies for ethanol decomposition intermediates on Pt(111) as calculated by the scaling relation based on data on Ru(0001)[39] (*x*-axis) and direct density-functional theory calculation on Pt(111) (*y*-axis; from ref 30).

(49) Spiewak, B. E.; Shen, J.; Dumesic, J. A. *J. Phys. Chem.* **1995**, *99*, 17640.

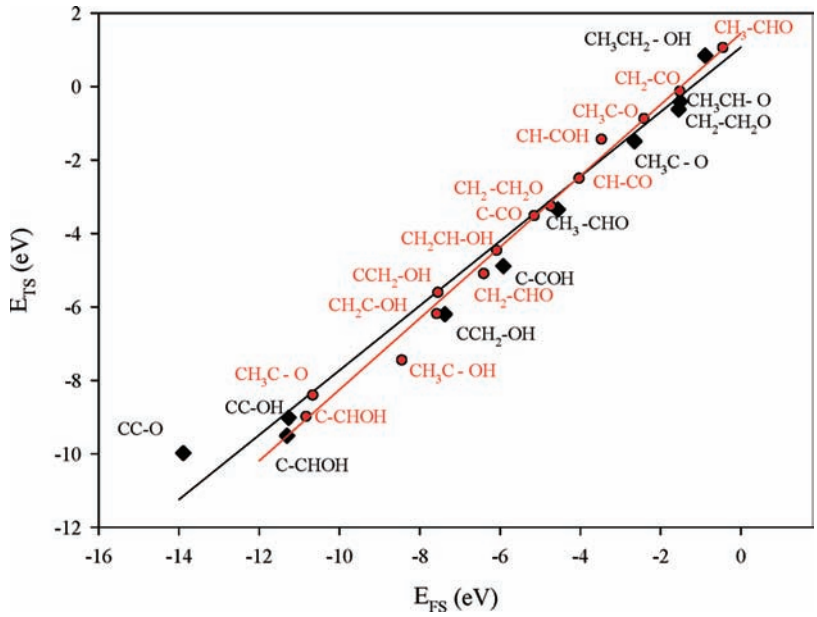

Figure 2. BEP correlation for C−C and C−O bond-breaking steps on Ru (0001)[39] (in black) and Pt(111)[30] (in red). The best fit line for Ru(0001) is E_{TS} (eV) = $0.88E_{FS} + 1.07$ ($R^2 = 0.98$), where E_{FS} is the energy of the final state for the reaction written in the exothermic direction, relative to the initial state gas-phase species and the clean slab. E_{TS} is the energy of the transition state with the same reference.

adsorbates and, second, the use of a BEP relation to predict the energetics of the transition state—allows us to map out the entire PES for the overall reaction on several metal surfaces. This mapping is done in Figure 3 for 10 relevant catalytic close-packed metal surfaces, where the energetics for C−C and C−O bond breaking in ethanol for all 24 possible C−C−O backbone intermediates on each of the 10 metals are shown. We note that this PES can be derived for any metal surface, provided that we know only the binding energy of CO, C, O, and H on that surface.

In principle, one could develop a full microkinetic model[50] based on this overall PES for each surface and use this model to predict the overall rate of this reaction, but one can see that even for this relatively simple system, the number of possible pathways is large. Additionally, this information is incomplete, as only direct C−O and C−C bond cleavages are given by the BEP relation considered here; for instance, disproportionation steps are not included in this analysis. In addition, C−H and O−H bond cleavage is not considered explicitly. While the use of the correlations as outlined above has vastly simplified the generation of large amounts of data, the challenge of extracting reaction rates from this data remains. As a first approximation, we have developed a simple mean-field kinetic model, as described below, to estimate reaction rates at steady state.

Surface Intermediates. Energetics for species included in the kinetic model were calculated as described above using the scaling correlation[28] and the DFT-calculated binding energies of H, C, O, and CO. The energy of the transition state is calculated from the BEP correlations developed on Ru(0001), as shown in Figure 2. The vibrational frequencies for all surface intermediates are calculated on Ru(0001);[39] these values are assumed to be independent of metal. Using these vibrational frequencies, we calculate the entropy and zero-point energies of surface species. Since vibrational frequencies are assumed to be independent of metal, both entropy and zero-point energies for surface species are also assumed to be independent of metal. Additionally, these two quantities are assumed to be invariant with surface coverage. Entropy values for gas-phase intermediates are taken from published tables.[51]

The model assumes the presence of a most abundant surface intermediate (MASI). To determine the nature of the MASI, all intermediates are first assumed to be in equilibrium with the appropriate gas-phase species and the stoichiometric amount of gas-phase hydrogen: $CH_xCH_yOH_z$ species are assumed to be in equilibrium with ethanol, CH_xCH_y species with ethane, CH_xOH_y species with carbon monoxide, CH_x species with methane, and OH_x species with water. The coverage of each species is calculated on the basis of this equilibrium, and the highest-coverage species is assigned as the MASI. The gas-phase pressure of each species is set equal to the value determined by the respective experimental measurement.

Our model includes the effect of surface coverage on the binding energy of reactive intermediates. In particular, we find that, under our experimental conditions, CO is the most abundant surface intermediate for all metals studied experimentally, except for Cu. For this reason, CO binding is calculated separately, rather than as a function of C binding on metal surfaces. As a first approximation for adsorbate binding energy as a function of CO surface coverage, we use a correlation developed earlier for Pt(111):[10]

$$\mathrm{BE_{CO}}(\theta_{CO}) = -1.78 + 0.0065e^{4.79\theta_{CO}} + 0.031135\theta_{CO}e^{4.79\theta_{CO}}$$

where BE_{CO} (eV) is the differential binding energy of CO (i.e., the binding energy of the last CO added to the surface), evaluated at the CO coverage of θ_{CO}. This correlation reflects the repulsive interaction between CO molecules on Pt(111) and accurately predicts the saturation coverage of CO on that surface. To a first approximation, we assume that the CO binding energy dependence on θ_{CO} on other transition metals is identical to that on Pt(111). In that case, the constant term in the above relation changes from metal to metal, depending on the initial binding energy of CO on that metal, but the second and third terms are kept invariant across the metals studied. Using this function, we can solve for the coverage of CO, which is the MASI for most metals studied. For Cu, where the majority of the surface is comprised of vacant sites, no coverage effects have been included in our analysis.

As the coverage of CO will also destabilize other surface species, we have included this effect in the model. To a first approximation,

(50) Cortright, R. D.; Dumesic, J. A. *Adv. Catal.* **2002**, *46*, 161.

(51) Afeefy, H.; Liebman, J. F.; Stein, S. E. *NIST Chemistry Webbook, NIST Standard Reference Database 69*; Linstrom, P. J., Mallard, W. G., Eds.; National Institute of Standards and Technology: Gaithersburg, MD.

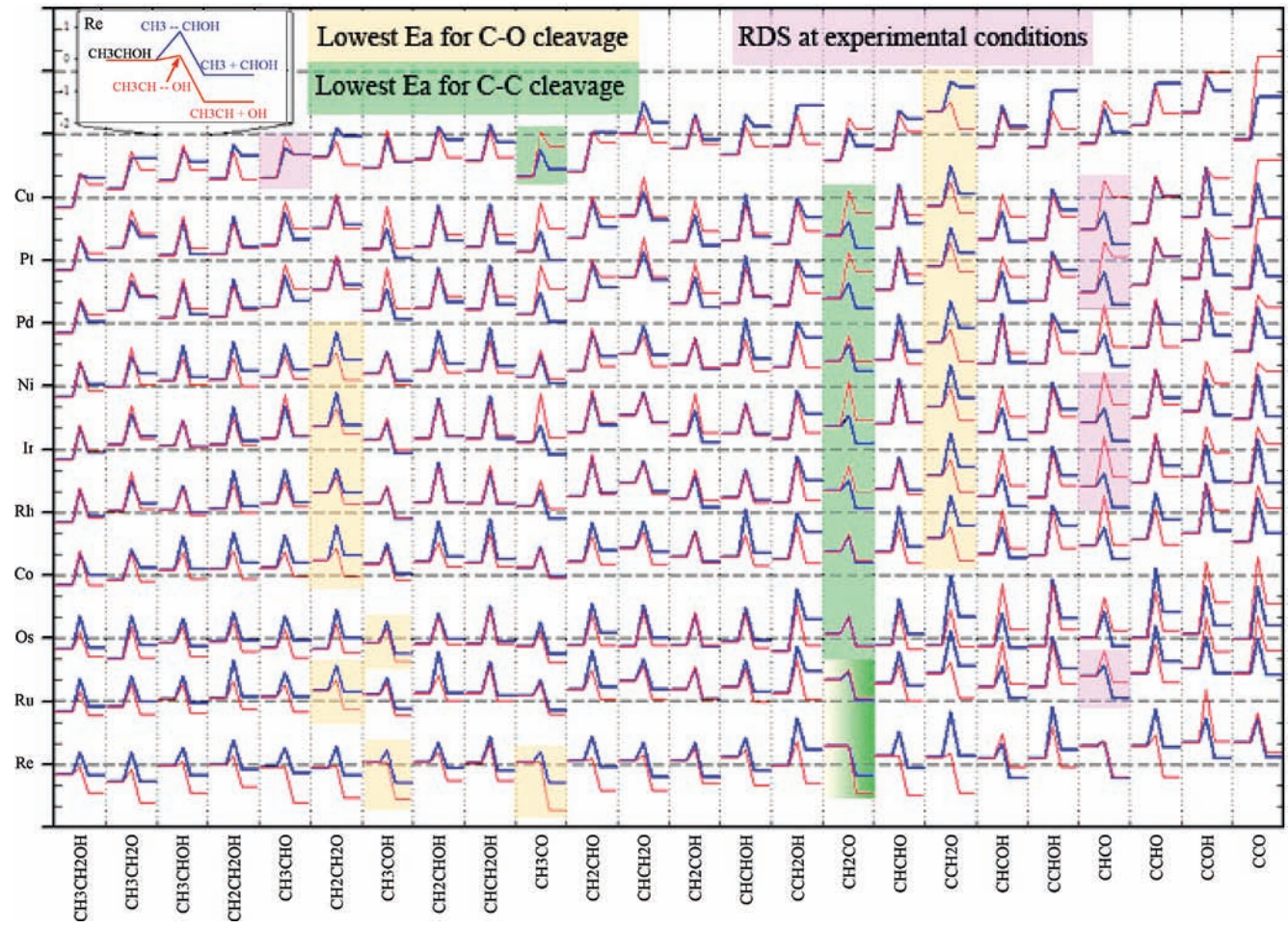

Figure 3. Potential energy surface for C−C and C−O bond-breaking in $CH_xCH_yOH_z$ ($x = 0-3$, $y = 0-2$, $z = 0-1$) on the close-packed surface of 10 transition metals. C−C cleavage is shown in blue; C−O cleavage is shown in red. Each tick-mark on the *y*-axis represents 1 eV. *x*-Axis labels give the intermediate where the C−C or C−O cleavage is taking place. The transition state is depicted by the top of each spike, whereas the initial and final state for each elementary step is indicated by the respective horizontal segments bracketing each spike. Background color indicates that the elementary step has an activation energy within 0.03 eV of the lowest activation energy (E_a) for C−C cleavage (green) and C−O cleavage (orange) for each metal. Purple background identifies the rate-determining step (RDS) for C−C cleavage as calculated by the kinetic model under the experimental conditions. Dual background color indicates that the respective intermediates fulfill both criteria represented by the respective colors. Inset: example detail for C−C and C−O cleavage in CH_3CHOH on Re.

we assume that the destabilization of other species due to the presence of CO will be similar to the destabilization of CO on itself.

Transition States. The energy of each transition state for C−C and C−O bond breaking is calculated using the BEP correlation developed on the Ru(0001) surface described above (see Figure 2). The final state energies, destabilized by the MASI (CO) as described above, are used to calculate the respective transition state energies. Entropy and zero-point energies of the transition states are assumed to be similar to those of the corresponding $CH_xCH_yOH_z$ surface species. It is also assumed according to transition state theory that there exists an equilibrium coverage of the most stable transition state with respect to gas-phase ethanol and hydrogen in the presence of the most abundant surface intermediate, calculated in the same manner as the surface intermediates described above.

Catalytic Activity. The rate of the overall reaction (either C−O or C−C bond-breaking) is assumed to be

$$R = A\theta_{TS}\theta_{vacant}$$

where A is the preexponential factor, R represents the turnover frequency (rate per site) of the reaction, θ_{TS} is the transition state coverage calculated as above, and θ_{vacant} is the coverage of vacant sites, calculated as one minus the coverage of the most abundant surface intermediate. This formulation assumes that the reaction requires two sites to take place, as the final state of the bond-breaking event delivers two intermediates on the surface. This assumption is in line with our observations from detailed calculations of ethanol decomposition on Ru(0001). In addition, the preexponential factor is assumed to be 10^{13} s^{-1} for all surface reactions. In this simple model, only the transition state with the highest coverage is assumed to contribute to the overall reaction rate; no secondary reaction channels are considered for ethanol decomposition. Using the most stable transition state, we calculate the rate of C−O cleavage and C−C cleavage.

Effect of Steps. Previous work has shown that, at least on certain metals, the decomposition of ethanol is structure-sensitive.[38] To probe the effects of structure sensitivity, we looked at the thermochemistry of CO dissociation on stepped (211) surfaces at the reaction temperature for the six metals studied experimentally. The results are shown in Table 2. CO dissociation on steps is favorable under our reaction conditions on Ru, Rh, and Ir; however, CO dissociation is less likely on Pt, Pd, and Cu steps. Thus, the steps on Pt, Pd, and Cu are unlikely to be poisoned by the products of CO dissociation (C and O), while Ru, Rh, and Ir are more likely to have their steps blocked by C and/or O. Since step sites on Pt, Pd, and Cu are likely free to catalyze this reaction, but equivalent sites on Ru, Rh, and Ir are unlikely to do the same, we need to include the effect of these sites on the former three metals but not

Table 2. Thermochemistry of CO Dissociation on the Face-Centered Cubic (211) Surfaces of the Metals Tried Experimentally for Ethanol Decomposition[a]

metal	ΔE of CO dissociation on step	ΔG of C + O binding on step at 523 K
Cu	1.77	2.70
Pt	0.37	1.30
Pd	1.78	2.71
Ir	−1.07	−0.14
Rh	−1.12	−0.19
Ru	−1.62	−0.69

[a] ΔE and ΔG represent total energy and Gibbs free energy change, respectively. All values are in eV. On Ru, an fcc structure was assumed to maintain a similar structure across metals.

Table 3. Experimental Results and Model Predictions for C−C and C−O Bond-Breaking Turnover Frequencies (TOF)

	experimental TOF (min^{-1})		model TOF (min^{-1})	
metal	C−C cleavage	C−O cleavage	C−C cleavage	C−O cleavage
Cu	∼0	∼0	2.4×10^{-4}	3.3×10^{-6}
Pt	1.1	0.022	53	6.8×10^{-14}
Pd	0.52	0.002	23	4.7×10^{-14}
Ir	0.21	0.013	31	4.6×10^{-10}
Rh	0.95	0.002	164	8.9×10^{-6}
Ru	2.6	0.021	115	0.35

on the latter. Due to their undercoordination, step sites generally stabilize intermediates and transition states as compared with close-packed surface sites. Work done by Vang et al.[52,53] has estimated the stabilization of the transition state for C−C cleavage on Ni steps to be about ∼0.4 eV. As a first approximation for the effect of steps on ethanol decomposition on these metals, we include an equivalent stabilization of the TS for C−C and C−O bond breaking on Pt, Pd, and Cu. Furthermore, steps will also increase the binding energy of the MASI significantly. This effect is included by calculating the binding energy of CO on a (211) surface and then applying the coverage-dependent destabilization as described for the (111) surface. Zero-point energy and entropy corrections are assumed to be similar to that of the (111) surface. The step density (used to adjust the pre-exponential factor) is assumed to be 5%.[54] Thus, the rate of reaction on stepped surfaces becomes

$$R = \rho_{step} A \theta_{TS} \theta_{vacant}$$

where ρ_{step} is the step density, A is the preexponential factor (as above), θ_{TS} is calculated as for the (111) surface, but adjusted for the stabilization of the transition state on the stepped surface, and θ_{vacant} is calculated as for the (111) surface but also adjusted for the stabilization of the MASI on the stepped surfaces.

The result of these simplifications is a model that depends on the experimental conditions (partial pressures of appropriate gas-phase species and temperature) and the calculated binding energy of only four intermediates (CO, C, O, and H) on the appropriate metal surfaces.

Results

The results from experimental measurements of ethanol conversion (see Tables 1 and 3) show that for five of the six metals tested the rate of ethane (C_2H_6) formation (via C−O bond cleavage) is at least 1−2 orders of magnitude lower than that of CH_4 and CO production (via C−C bond cleavage). This result is predicted well by our model, where C−C bond cleavage is significantly favored on these surfaces. On Cu, neither CH_4 nor CO nor C_2H_6 was observed in the effluent stream. The rates of C−O and C−C cleavage on Cu are both predicted to be very low, because of the low stability of all intermediates and the related transition states on this metal.

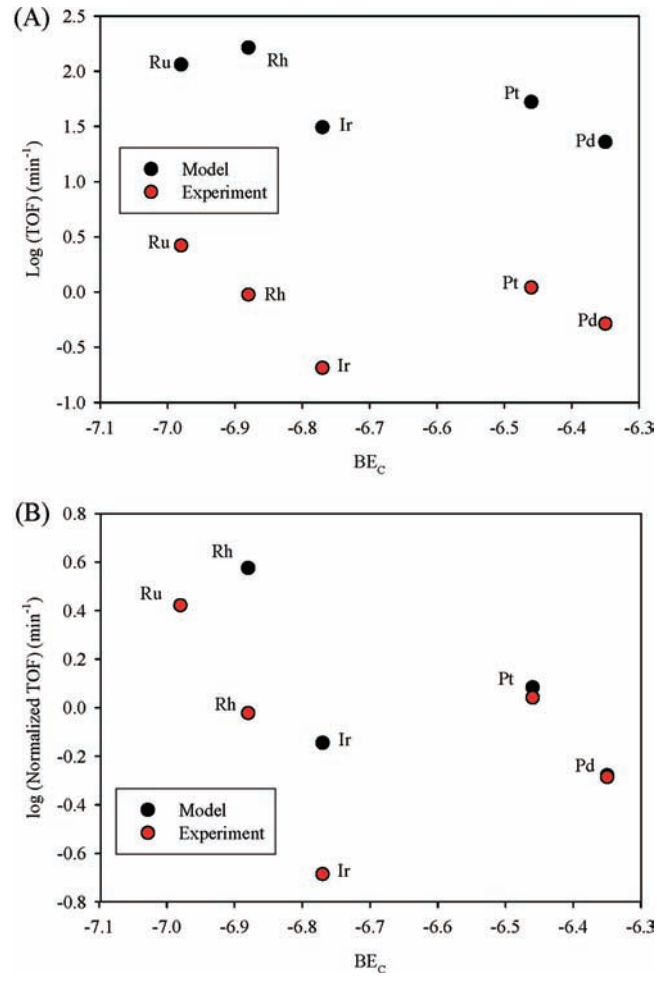

Figure 4. (A) log of experimental and model-predicted TOFs (in min^{-1}) for C−C bond-breaking in ethanol. (B) log of experimental and normalized-model predicted TOFs (Normalization factor for model rates is the experimental rate on Ru divided by the model rate on Ru). By definition, the model and experimental points for Ru are identical; the respective points on Pd are also very similar. The *x*-axis is the binding energy of carbon (in eV) on the close-packed surface as calculated by direct DFT. Both the model-predicted and the experimental TOF for ethanol decomposition on Cu are negligible.

The selectivity toward C−C cleavage on all the five active metals studied here results from the relatively weak bonding of O as compared with C on these surfaces. Since the final state of any C−O cleavage contains a species bound through oxygen, the lower O binding on these surfaces means that, in general, the final state (and therefore the transition state, through the BEP relation) is destabilized for C−O cleavage compared to C−C cleavage. This behavior also provides an indicator of what type of metal would be better able to selectively break the C−O bond: one with O binding closer to that of C binding.

The experimental rate (given as TOF) for C−C bond breaking together with the model prediction for each catalyst tested is given in Table 3 and Figure 4A. In every case, except Cu (where

(52) Vang, R. T.; Honkala, K.; Dahl, S.; Vestergaard, E. K.; Schnadt, J.; Laegsgaard, E.; Clausen, B. S.; Nørskov, J. K.; Besenbacher, F. *Nat. Mater.* **2005**, *4*, 160.
(53) Vang, R. T.; Honkala, K.; Dahl, S.; Vestergaard, E. K.; Schnadt, J.; Laegsgaard, E.; Clausen, B. S.; Nørskov, J. K.; Besenbacher, F. *Surf. Sci.* **2006**, *600*, 66.
(54) Dahl, S.; Sehested, J.; Jacobsen, C. J. H.; Tornqvist, E.; Chorkendorff, I. *J. Catal.* **2000**, *192*, 391.

both predicted and experimental rates are negligible), the TOF predicted by the model is approximately 2 orders of magnitude higher than the value from experiment. This overprediction is not unexpected, given the assumptions made by the model and the uncertainty in DFT and the correlations used, as noted above. However, if trends, rather than absolute rates, are compared across catalysts, the correlation between experiment and model rates is much better. Figure 4B gives the model TOF normalized to the experimental TOF on Ru. The results show that the model predicts the relative TOF of each metal to within half an order of magnitude in all cases, a remarkable result given the numerous simplifying assumptions used in developing this model.

The results from the above simple model also yield significant information regarding the reaction pathway. For example, on all metals used in this study, except Cu, under the selected experimental conditions, the predicted rate-determining step (RDS) for C−C cleavage is the same, namely cleavage through the CH−CO intermediate (see Figure 3). This intermediate has been proposed previously for this reaction on Pt[30] and Ir[42] at similar temperatures.

Conclusion

By combining Brønsted-Evans-Polyani correlations developed for C−C and C−O cleavage with the scaling relations developed by Abild-Pedersen and colleagues, we have generated the entire potential energy surface for ethanol decomposition on several transition metals, whereby DFT calculations are used only to calculate a minimum number of quantities, namely, the binding energy of C, O, H, and CO on each metal. Using the potential energy surface developed in this way, we then constructed a simple kinetic model to provide qualitative trends in activity and selectivity for ethanol decomposition. Despite the simplicity of the model, trends among model-predicted rates are in good agreement with experimental reaction rate trends measured on six supported metal catalysts.

The reduction of the ethanol decomposition potential energy surface across transition metals to just a few binding energy calculations illustrates a significant speed-up in (i) mining for reactivity trends among catalysts and (ii) utilizing first-principles-based catalyst design efforts for more complicated reaction networks.

Acknowledgment. J.K.N. acknowledges Hougen Professorship funds from the University of Wisconsin—Madison, Department of Chemical & Biological Engineering. This work was funded by the US Department of Energy, Office of Basic Energy Sciences, Division of Chemical Sciences. Research was performed in part using supercomputing resources at the following institutions: (1) EMSL, a national scientific user facility located at Pacific Northwest National Laboratory; (2) the National Center for Computational Sciences (NCCS) at Oak Ridge National Laboratory; (3) the Center for Nanoscale Materials (CNM) at Argonne National Laboratory; and (4) the National Energy Research Scientific Computing Center (NERSC). EMSL is sponsored by the US Department of Energy's Office of Biological and Environmental Research. NCCS, CNM, and NERSC are supported by the Office of Science of the US Department of Energy under Contract No. DE-AC05-00OR22725, DE-AC02-06CH11357, and DE-AC02-05CH11231, respectively.

JA8099322